

# Mantle Dynamics in Super-Earths: Post-Perovskite Rheology and Self-Regulation of Viscosity

<sup>1</sup>P. J. Tackley, <sup>2</sup>M. Ammann, <sup>2</sup>J. P. Brodholt, <sup>2</sup>D. P. Dobson, <sup>3</sup>D. Valencia

<sup>1</sup>Institute of Geophysics, ETH Zurich, Sonneggstrasse 5, Zurich, 8092 Switzerland  
(ptackley@ethz.ch; Tel: +41 446332758, Fax: +41 446331065)

<sup>2</sup>Department of Earth Sciences, University College London, Gower Street, London WC1E 6BT, UK

<sup>3</sup>Department of Earth, Atmospheric and Planetary Sciences, Massachusetts Institute of Technology, Cambridge MA 02139, USA

## Abstract

The discovery of extra-solar "super-Earth" planets with sizes up to twice that of Earth has prompted interest in their possible lithosphere and mantle dynamics and evolution. Simple scalings suggest that super-Earths are more likely than an equivalent Earth-sized planet to be undergoing plate tectonics. Generally, viscosity and thermal conductivity increase with pressure while thermal expansivity decreases, resulting in lower convective vigor in the deep mantle, which, if extrapolated to the largest super-Earths might, according to conventional thinking, result in no convection in their deep mantles due to the very low effective Rayleigh number. Here we evaluate this. First, as the mantle of a super-Earth is made mostly of post-perovskite we here extend the density functional theory (DFT) calculations of post-perovskite activation enthalpy of to a pressure of 1 TPa, for both slowest diffusion (upper-bound rheology) and fastest diffusion (lower-bound rheology) directions. Along a 1600 K adiabat the upper-bound rheology would lead to a post-perovskite layer of a very high ( $\sim 10^{30}$  Pa s) but relatively uniform viscosity, whereas the lower-bound rheology leads to a viscosity increase of  $\sim 7$  orders of magnitude with depth; in both cases the deep mantle viscosity would be too high for convection. Second, we use these DFT-calculated values in numerical simulations of mantle convection and lithosphere dynamics of planets with up to ten Earth masses. The models assume a compressible mantle including depth-dependence of material properties and plastic yielding induced plate-like lithospheric behavior. Results confirm the likelihood of plate tectonics for planets with Earth-like surface conditions (temperature and water) and show a novel self-regulation of deep mantle temperature. The deep mantle is not adiabatic; instead feedback between internal heating, temperature and viscosity regulates the temperature such that the viscosity has the value needed to facilitate convective loss of the radiogenic heat, which results in a very hot perovskite layer for the upper-bound rheology, a super-adiabatic perovskite layer for the lower-bound rheology, and an azimuthally-averaged viscosity of no more than  $10^{26}$  Pa s. Convection in large super-Earths is characterised by large upwellings (even with zero basal heating) and small, time-dependent downwellings, which for large super-Earths merge into broad downwellings. In the context of planetary evolution, if, as is likely, a super-Earth was extremely hot/molten after its formation, it is thus likely that even after billions of years its deep interior is still extremely hot and possibly substantially molten with a "super basal magma ocean" – a larger version of the proposal of (Labrosse et al., 2007), although this depends on presently unknown melt-solid density contrast and solidus.

**Keywords:** extrasolar planet; terrestrial planets; tectonics; interiors

## 1. Introduction

There is much interest in the possible structure and dynamics of large rocky planets (super-Earths) around other stars, which may exist around as many as 23% of stars (Howard et al., 2010). Initial studies focused on determining the radial structure of such planets (Seager et al., 2007; Sotin et al., 2007; Valencia et al., 2006; Valencia et al., 2007b; Valencia et al., 2007c).

A first-order question is whether super-Earths are likely to experience plate tectonics, and this has so far been approached using simple models. Boundary-layer theory, taking into account the increase in mean density with planet size (Valencia and O'Connell, 2009; Valencia et al., 2007a) predicts that plate tectonics becomes more likely with increasing planet size; recent dynamical calculations and theory support this (Korenaga, 2010a; van Heck and Tackley, 2011). While one study finds the opposite conclusions (O'Neill and Lenardic, 2007), it is argued in (van Heck and Tackley, 2011) that this might be a consequence of working in nondimensional space and not scaling all nondimensional parameters in a consistent manner with planet size.

In general, viscosity and thermal conductivity increase with pressure while thermal expansivity decreases with pressure, all of which result in lower convective vigour in the deep mantle, which several studies have shown to result in large-scale structures in Earth's deep mantle (e.g. (Balachandar et al., 1992; Hansen et al., 1991; Hansen et al., 1993)). The pressure at the core-mantle boundary (CMB) of a ten Earth mass super-Earth is about ten times the pressure at Earth's CMB (Valencia et al., 2009), so if these trends in physical properties continue, a super-Earth's deep mantle would be expected to have a very low effective Rayleigh number and therefore, according to classical ideas, very sluggish or no convection (e.g. (Stamenković et al., 2011)). Stamenković et al. (2012) found using 1-D and 2-D models with an estimated perovskite rheology that in fact the heat transport mode and viscosities depend on initial temperatures and time. The purpose of this study is to investigate the thermal, rheological and convective state with a post-perovskite rheology calculated using density functional theory (DFT).

Dynamical studies to date have generally not taken into account these large changes in viscosity, thermal expansivity and thermal conductivity with pressure. An exception is the study of (van den Berg et al., 2010), who focussed on the influence of variable thermal conductivity on convection in super-Earths that are undergoing stagnant lid convection, finding that large thermal conductivity in the deep mantle results in strong coherent upwellings from the core-mantle boundary. They found that the temperature eventually adopts an adiabatic profile, as is normally found in convective systems. While they also included pressure-dependence of viscosity and thermal expansivity, they did not analyse their effects. Another exception is the study of (Stamenković et al., 2012), who used 1-D parameterized and 2-D convection models to investigate the influence of a strong increase in activation enthalpy with pressure, although they used average scalings for thermal expansivity and thermal conductivity.

Complicating the extrapolation of physical properties to higher pressure is the possible influence of phase transitions. The perovskite (Pv) to post-perovskite (pPv) transition, occurring at a pressure of around 125 GPa, is well-established. An important issue is whether post-perovskite remains stable to ~1400 GPa, which is the pressure at the base of the largest super-Earth's mantle. First-principles calculations by (Umamoto et al., 2006) indicated that MgSiO<sub>3</sub> post-perovskite may break down into constituent oxides (MgO+SiO<sub>2</sub>) at around 1000 GPa. Recent laboratory experiments on the analog material NaMgF<sub>3</sub>, however, questioned

101 this finding (Grocholski et al., 2010). Thus, for the purposes of this initial study, we assume  
102 that post-perovskite is the stable phase to the base of a super-Earth mantle.

103  
104 The physical properties of post-perovskite are still being evaluated. Its viscosity is highly  
105 anisotropic. Ammann et al. (2010b) used density functional theory (DFT) to calculate  
106 activation enthalpies for the different diffusion directions, finding differences of several orders  
107 of magnitude between them. Based on physical arguments they argue that diffusion creep will  
108 be controlled by the slowest diffusion direction while dislocation creep could be controlled by  
109 that the easiest diffusion direction, concluding that in this case the viscosity of post-perovskite  
110 could be 2-3 orders of magnitude lower than that of perovskite at the same pressure and  
111 temperature.

112  
113 While study of (Ammann et al., 2010b) focussed on the pressure range of Earth's mantle, a  
114 key question for super-Earths is how the viscosity changes at up to 10 times this pressure.  
115 Thus, in this study we have extended these DFT calculations to calculate activation enthalpies  
116 for diffusion creep in post-perovskite at pressures of up to 1 TPa. These values are then used  
117 in dynamical calculations of mantle convection in super-Earths that also include reasonable  
118 physical variations of other parameters and yielding-induced plate tectonics. It has recently  
119 been argued that at very high pressures, deformation by interstitial diffusion may become  
120 more effective than by vacancy diffusion, possibly even causing in a decrease of viscosity  
121 with pressure along an adiabat (Karato, 2011). At present this possibility is not quantified so  
122 we will leave it to a future study.

## 123 124 **2. Rheology**

### 125 126 **2.1 Density Functional Theory calculations**

127  
128 Here we perform density functional theory (DFT) calculations of vacancy diffusion in post-  
129 perovskite using the method described in (Ammann et al., 2008, 2010a; Ammann et al.,  
130 2010b). Full details and accuracy tests are given in Ammann et al. 2010b (main paper and  
131 supplementary material); here summarise the main points. The viscosity of post-perovskite,  
132 assuming diffusion creep, is controlled by magnesium diffusion and the effective diffusivity,  
133  $D_{\text{eff}}$ , which limits the rate of deformation, can be well approximated by  $D_{\text{eff}}=5D_{\text{Mg}}$ . The large  
134 anisotropy in diffusion implies a large viscosity spectrum lying somewhere between the two  
135 extremal cases of diffusion along x (lower bound) and along y (upper bound). We write the  
136 viscosity  $\eta$  as follows:

$$137 \eta = \eta_0 \frac{G^2 k_J T}{N_v} \exp\left(\frac{H}{kT}\right) \quad (1)$$

138  
139 Here,  $G$  is the characteristic grain size (in the Earth's lower mantle somewhere between 0.1-1  
140 mm),  $N_v$  is magnesium-vacancy concentration (in the lower mantle estimated to be around  
141  $10^{-7} - 10^{-3}$ ),  $H$  is the migration enthalpy (given in the table below in eV) and  $k$  is Boltzmann's  
142 constant ( $8.617343 \cdot 10^{-5}$  eV). Grain size and vacancy concentrations are chosen such that they  
143 well reproduce lower mantle viscosity profiles (Ammann et al., 2010a) and are assumed to be  
144 similar in post-perovskite (Ammann et al., 2010b); a similar vacancy concentration is  
145 expected if, as seems probable, vacancies are mostly extrinsic rather than intrinsic. The  
146 prefactor is given by  $\eta_0 = 1/(5\alpha \cdot 2/3 \cdot l^2 \nu V_{\text{mol}})$  and is listed in Table 1.  $\alpha$  is a geometrical factor  
147 ( $40/3$  or  $16/3$  with or without grain boundary sliding respectively, the former was used here),  $l$   
148 is the jump distance,  $V_{\text{mol}}$  is the molecular volume and  $\nu$  is the attempt frequency times the  
149 exponential of the migration entropy (see (Ammann et al., 2010a; Ammann et al., 2010b) for  
150 details). Magnesium diffuses along y via six-jump cycles on the magnesium-silicon sublattice  
151

152 (Ammann et al., 2010b). For simplicity, we approximate the six different jumps as one single  
153 jump with an effective migration enthalpy,  $H^{\text{high}}$ , and attempt frequency (included in  $\eta_0$ ). For  
154 magnesium diffusion along  $x$ , the fast direction, no such simplification had to be made.

155 The accuracy of this method was discussed and tested in Ammann et al. (2010b)  
156 (supplementary information). Assuming that the difference between LDA (Local Density  
157 Approximation) and GGA (Generalized Gradient Approximation) values provides an  
158 estimate of the DFT uncertainties, then the energies are correct to within about 10%. The  
159 effect of modelled system size was assessed by calculating the migration enthalpies in a  
160  $3 \times 1 \times 1$  and a larger  $3 \times 1 \times 2$  supercell, and the values found to differ by less than 5% (in some  
161 cases less than 1%) between the two system-sizes (Ammann et al. 2010b supplementary  
162 information). System-size effects were investigated in more detail for periclase in Ammann et  
163 al. (2012); it was found that migration enthalpies change with system size non-linearly and  
164 are already converged to an accuracy of around 10% even in small cells, further supporting  
165 the 5% estimated cell-size effect in the present calculations.

166

## 167 **2.2 Analytical fit**

168

169 In order to insert  $H(p)$  for post-perovskite and perovskite into convection calculations, it is  
170 necessary to fit the DFT-calculated values to an analytical expression. After trying theoretical  
171 (e.g. elastic strain energy model) and *ad hoc* analytic forms, the following was found to give a  
172 good fit:

173

$$174 \quad H(p) = E_0 + pV(p) \quad (2)$$

$$175 \quad V(p) = V_0 \exp\left(-\frac{p}{p_{\text{decay}}}\right) \quad (3)$$

176

177 This was fit to the data in (Ammann et al., 2008) for perovskite and to both the upper-bound  
178 and lower-bound data in Table 1 for post-perovskite. For the pressure range of Earth's upper  
179 mantle an olivine rheology is assumed (Karato and Wu, 1993). The resulting fit of  $H(p)$  is  
180 plotted in Figure 1(a) and the relevant parameters are given in Table 2. Clearly, the effective  
181 activation volume decreases with pressure and is very low for post-perovskite, dropping over  
182 the considered pressure range from about 1.5 to 0.5  $\text{cm}^3/\text{mol}$  for the upper-bound rheology  
183 and 1.3 to 0.6  $\text{cm}^3/\text{mol}$  for the lower-bound rheology. This is slightly lower than predicted by  
184 (Wagner et al., 2011). Considering total enthalpy, the estimates of Stamenković et al (2011)  
185 are within our bounds below 700 GPa, and above 700 GPa are at most 20% larger than our  
186 results.

187

## 188 **3. Convection Models**

189

### 190 **3.1 Physical model and numerical method**

191

#### 192 *3.1.1 Viscosity*

193

194 Diffusion creep is assumed to be the dominant deformation mechanism, and is assumed to  
195 follow an Arrhenius law:

196

$$197 \quad \eta(T, p) = \eta_0 \exp\left[\frac{H(p)}{RT} - \frac{H(0)}{RT_0}\right] \quad (4)$$

198

199 where  $H(p)$  is given by equations (2)-(3),  $\eta_0$  is the reference viscosity obtained at zero  
200 pressure and reference temperature  $T_0$ , which is chosen to be 1600 K. As mentioned in section  
201 2.2, an olivine rheology is assumed for the pressure range of Earth's upper mantle, a  
202 perovskite rheology is assumed in the perovskite stability field and a post-perovskite rheology  
203 is used for higher pressures. For perovskite,  $\eta_0$  is calculated so as to give a factor 10 viscosity  
204 increase from the upper mantle to the lower mantle, while for post-perovskite  $\eta_0$  is calculated  
205 so as to give either a factor  $10^5$  viscosity increase (for the upper bound pPv rheology) or factor  
206 100 viscosity decrease (for the lower bound pPv rheology) at the pV-pPv transition. The  
207 former increase is consistent with Ammann et al. (2010b) while the decrease is somewhat less  
208 than the 4-5 orders of magnitude estimated in Ammann et al. (2010b) in order to be  
209 conservative regarding the possible weakness of pPv. For this initial study, viscosities in  
210 Earth's mantle's pressure range are about 2 orders of magnitude higher than realistic, with  
211 upper mantle  $\eta_0=10^{21}$  Pa s (resulting values for other phases are listed in Table 2), in order to  
212 allow us to resolve convection in a super-Earth with reasonable computational resources.

213  
214 As discussed in Ammann et al. (2010b), diffusion creep is likely to be controlled by the upper  
215 bound rheology; thus we perform a suite of simulations using this. For the sake of  
216 comparison, we also perform simulations with the lower bound rheology, which may be  
217 relevant to dislocation creep (although for simplicity we here use a linear stress-strain rate  
218 relationship for both bounds).

219  
220 Illustrative resulting viscosity profiles for upper mantle  $\eta_0=10^{21}$  Pa s calculated along an  
221 adiabat with a 1600 K potential temperature (see next section for relevant physical properties)  
222 are plotted in Figure 1(b). Interestingly, while the upper-bound pPv viscosity is extremely  
223 high at  $>10^{30}$  Pa s, it remains approximately constant with pressure, first increasing by  $\sim 1$   
224 order of magnitude then decreasing by  $\sim 2$  orders of magnitude. This is because the viscosity  
225 depends on the ratio  $H(p)/T_{\text{adiabat}}(p)$ , and the adiabatic temperature increases in about the same  
226 proportion with pressure as  $H(p)$ . Nevertheless, convection would not take place if the  
227 viscosity were this high. The lower-bound pPv viscosity, in contrast, increases by  $\sim 7$  orders of  
228 magnitude along an adiabat from 130 to 1400 GPa. With the assumed absolute viscosities this  
229 results in a viscosity of  $\sim 10^{30}$ - $10^{31}$  Pa s near the CMB in a  $10 M_E$  super-Earth, which would be  
230 enough to stop convection in this region. Even so, this is a much lower increase than the  $\sim 15$   
231 orders of magnitude predicted by (Stamenković et al., 2011) based on perovskite rheology  
232 extrapolated using simple laws. It is possible that a larger viscosity increase than we predict  
233 could occur if extrinsic vacancy concentration decreases with pressure, due to changes in  
234 element partitioning or growth of a new phase, whereas we assume a constant extrinsic  
235 vacancy concentration. However, there is currently little experimental evidence that extrinsic  
236 vacancies change significantly with pressure. Nevertheless, one must accept that that vacancy  
237 concentrations in super-Earths are uncertain. Larger diffusion-creep viscosities would also  
238 occur if grain size becomes larger at higher pressure because the higher temperatures cause  
239 more rapid grain growth, as suggested by (Stamenković et al., 2011).

240  
241 This difference in the pressure scaling of lower- and upper-bound viscosities is due to  
242 anisotropic compression of the lattice. Diffusion in the 100 and 001 directions requires  
243 dilation in the 101 direction. This is the most compressible direction and so with pressure  
244 will become stiffer quicker than in the other two directions. Thus, increasing pressure slows  
245 diffusion in the 100 and 001 directions to a greater extent than diffusion in the 010 direction  
246 (the slowest one). Note that the "lower-bound" viscosity assumed here is 2-3 orders of  
247 magnitude higher (compared to Pv) than predicted in Ammann et al. (2010b) in order to be  
248 conservative; if we plotted the latter then it would always be substantially lower than the  
249 upper-bound viscosity. If the lower bound is relevant to dislocation creep, then the power-law  
250 rheology associated with dislocation creep would likely further reduce the viscosity increase,

251 because Christensen (1984) showed that power-law rheology can be approximated by  
 252 Newtonian rheology with its activation enthalpy reduced by factor  $n$ , the power-law index.  
 253

254 Plastic yielding occurs at high stresses, giving a first-order approximation of plate tectonics  
 255 (Moresi and Solomatov, 1998; Tackley, 2000; Trompert and Hansen, 1998). The pressure-  
 256 dependent yield stress is given by a combination of brittle and ductile processes as:  
 257

$$258 \quad \sigma_Y = \min\left(c_f p, \sigma_{duct} + \sigma'_{duct} p\right) \quad (5)$$

259  
 260 where  $c_f$  is the Byerlee's law friction coefficient,  $\sigma_{duct}$  is the ductile yield stress and  $\sigma'_{duct}$  is  
 261 the pressure gradient of ductile yield stress, which prevents yielding in the deep mantle.

262 Values are given in Table 4. For the smallest planet case,  $\sigma_{duct}$  had to be reduced by a factor  
 263 of 2 in order to avoid the stagnant lid mode of convection.  
 264

265 The effective viscosity, combining diffusion creep and plastic yielding, is given by:  
 266

$$267 \quad \eta_{eff} = \left( \eta_{diff}^{-1} + \frac{2\dot{\epsilon}}{\sigma_Y} \right)^{-1} \quad (6)$$

268  
 269 where  $\dot{\epsilon}$  is the second invariant of the strain-rate tensor.

270 Finally, the viscosity is truncated between  $10^{19}$  and  $10^{40}$  Pa s (using simple min and max  
 271 functions) in order to facilitate numerical solution.  
 272

### 273 3.1.2 Density

274  
 275 A Birch-Murnaghan third order equation of state is used to relate density to pressure and  
 276 calculate bulk modulus  $K$ . For simplification, rather than consider all mineral phases present  
 277 the mantle is divided into "upper mantle", "transition zone", "perovskite" and "post-  
 278 perovskite" mineralogies, with different parameters ( $K_0$ ,  $K'$  and  $Q_0$ ) for each, which are  
 279 chosen to match the widely-used Earth model PREM (Dziewonski and Anderson, 1981).  
 280 Obtained values are listed in Table 3 and the resulting density profile along the reference  
 281 adiabat is given in Figure 2b.  
 282

### 283 3.1.3 Thermal expansivity

284  
 285 The thermal expansivity depends on pressure and is given by:  
 286

$$287 \quad \alpha = \frac{\rho \gamma C_p}{K} \quad (7)$$

288  
 289 where the pressure-dependent density  $\rho$  and bulk modulus  $K$  are calculated as described  
 290 above, the specific heat capacity  $C_p$  is assumed constant, and Gruneisen parameter  $\gamma$  is given  
 291 by:  
 292

$$293 \quad \gamma = \gamma_0 \left( \frac{\rho_0}{\rho} \right) \quad (8)$$

294

295 This leads to the profile in Figure 2(c). The effect of Gruneisen parameter decreasing with  
296 density (pressure) is to give a stronger decrease of thermal expansivity with pressure, and  
297 therefore decrease the adiabatic temperature gradient, making the interior cooler (hence more  
298 viscous) than would be predicted with a constant Gruneisen parameter. Thermal expansivity  
299 decreases to about  $0.9 \times 10^{-5} \text{ K}^{-1}$  at Earth's CMB pressure, consistent with mineral physics  
300 constraints (Chopelas and Boehler, 1992; Katsura et al., 2010; Komabayashi et al., 2008;  
301 Mosenfelder et al., 2009), and to about  $1.5 \times 10^{-6} \text{ K}^{-1}$  at 1400 GPa, which appears to be  
302 consistent with that estimated by (Stamenković et al., 2011) using a completely different  
303 approach.

304

305 This leads to the adiabatic temperature profile given in Figure 2(a), in which a 1600 K surface  
306 temperature increases to  $\sim 2350 \text{ K}$  at Earth's CMB pressure and  $\sim 3630 \text{ K}$  at a  $10 M_{\text{E}}$  super-  
307 Earth's CMB. This corresponds to mean dissipation numbers (given by  $\log(T_{\text{cmb}}/T_{\text{surf}})$ ) of 0.38  
308 and 0.82, respectively. The dissipation number gives an indication of the importance of  
309 viscous dissipation and adiabatic heating in the global energy balance (Backus, 1975; Hewitt  
310 et al., 1975; Jarvis and McKenzie, 1980). Thus, despite the much higher pressure, these terms  
311 are only  $\sim$ twice as important as they are in Earth.

312

### 313 3.1.4 Thermal conductivity

314

315 The thermal conductivity is  $k = \rho C_p \kappa$ , where the thermal diffusivity  $\kappa$  is given by:

$$\kappa = \kappa_0 \left( \frac{\rho_0}{\rho} \right)^{-1} \quad (9)$$

316

317

318 This gives a moderate increase of  $k$  with pressure that is consistent with findings from a  
319 recent mineral physics study (de Koker, 2010) although other studies estimate higher values  
320 (Goncharov et al., 2009; Hofmeister, 2008). The surface value of  $k$  is  $3.0 \text{ W/K/m}$ , and over  
321 Earth's mantle's pressure range it increases to  $7.2 \text{ W/K/m}$ . This treatment does not include the  
322 radiative component. It is plausible that the radiative component might be important at the  
323 high temperatures obtained deep in super-Earths, but for simplicity it will not be considered in  
324 this initial study.

325

### 326 3.1.5 Constant properties and boundary conditions

327

328 Internal heating rate per unit mass is assumed constant, as is heat capacity  $C_p$ . Acceleration  
329 due to gravity  $g$  is also assumed to be constant but varies with planet size. In Earth's mantle  
330 this is a good approximation because  $g$  varies by only  $\sim 8\%$  according to PREM (Dziewonski  
331 and Anderson, 1981). In a  $10 M_{\text{E}}$  super-Earth  $g$  may change by a somewhat larger factor, but  
332 as this is smaller than the uncertainties in most other physical parameters, it is reasonable to  
333 ignore it and assume a constant value. This constant value is set so as to give the correct  
334 pressure at the CMB for a planet of a given size.

335

336 The surface is assumed to be isothermal with a temperature of  $300 \text{ K}$ , while the CMB is also  
337 assumed to be isothermal, with a temperature that is adjusted each time step to give zero net  
338 heat flow. Zero net CMB heat flow is an idealisation made for this initial study because we  
339 have no idea what the CMB temperature is in super-Earths: predicting this requires detailed  
340 modelling of their evolution from a hot initial state, which has so far been done only for  
341 isoviscous super-Earths (Kite et al., 2009; Papuc and Davies, 2008) – we plan in future to do  
342 this for super-Earths with pressure-dependent viscosity. In Earth, it is generally thought that  
343 heat from the core provides only a small fraction of the global heat budget (Davies and

344 Richards, 1992; Jaupart et al., 2007; Schubert et al., 2000), therefore this is a reasonable first-  
345 order approximation to ignore it. Both boundaries are mechanically free-slip.

346

### 347 *3.1.6 Planetary dimensions*

348

349 It is assumed that the relative masses of the mantle and core, as well as their compositions, are  
350 the same as those of the Earth. For a given planetary mass, the planetary radius, CMB radius  
351 and the average  $g$  for the mantle are calculated using a Matlab script that calculates a 1-D  
352 profile of the planet by integrating with pressure the equations given above, and iterating on  
353 planet size until the mass and size match. The results are in Table 5. These dimensions and  
354 the mean  $g$  are then used as input parameters for the convection calculations. These numbers  
355 are slightly different from those calculated by Valencia et al. (2006) because they assumed a  
356 pure iron core whereas here the parameters are tuned to match PREM (Dziewonski and  
357 Anderson, 1981). These differences are typically of order  $\sim$ few %; up to 9% for pressure at  
358 the CMB, which reflects the general uncertainty in calculating high-pressure properties and  
359 will not make a significant difference to the convection results presented here.

360

### 361 *3.1.7 Phase transitions*

362

363 Phase transitions are included, as in our previous studies for Earth (e.g. (Nakagawa and  
364 Tackley, 2005b, 2011; Tackley and Xie, 2003)), but we here set all Clapeyron slopes to zero  
365 in order to reduce the number of complexities influencing the convection; phase transitions  
366 thus influence only the radial density profile and the viscosity. The reader is referred to  
367 publications referenced above for full details on the assumptions and implementation. In  
368 brief: two sets of phase transitions are included: those for olivine and those for pyroxene-  
369 garnet, and it assumed that the mantle is 60% olivine and 40% pyroxene-garnet. Table 6 gives  
370 the included phase transitions. For super-Earths, depths are scaled inversely with mean  
371 gravitational acceleration listed in Table 5.

372

### 373 *3.1.8 Solution method*

374

375 The physical model is solved using the numerical code StagYY (Tackley, 2008) in a two-  
376 dimensional spherical annulus (Hernlund and Tackley, 2008). StagYY uses a finite-volume  
377 discretization of the governing compressible anelastic equations, and either a multigrid solver  
378 or a direct solver to obtain a solution. For the present calculations the direct solver  
379 UMFPACK (Davis, 2004) is used, and is accessed using the PETSc toolkit (Balay et al.,  
380 2012; <http://www.mcs.anl.gov/petsc>). For this study, dimensional units are used throughout  
381 because most nondimensional parameters involve the mantle depth  $D$  as the length scale, so  
382 changing planet size would result in almost all nondimensional parameters changing, but only  
383 a few dimensional parameters changing. For this initial study, calculations are run to a  
384 statistically steady-state, at which quantities such as heat flux, mean temperature and rms.  
385 velocity fluctuate about a mean value that does not have a secular change. This can take  
386 billions of years of simulated time. The numerical resolution depends on planet size: higher  
387 resolution is needed for larger planets. When a statistically steady-state is reached the solution  
388 is continued at twice the resolution in both directions in order to check that it does not change  
389 significantly. The highest resolution used was 128 points in radius by 1024 points in azimuth,  
390 with radial grid spacing decreased by a factor of 2-3 towards the surface in order to  
391 adequately resolve the lithosphere.

392

## 393 **3.2 Results**

394

### 395 *3.2.1 Upper bound rheology*



396

397 Figure 3 shows temperature and viscosity fields for all five planet sizes and the upper bound  
398 rheology. The existence of downwellings with a low temperature and high viscosity in all  
399 planet sizes indicate a mobile-lid tectonic mode, i.e. the lithosphere can "subduct". If instead  
400 the stagnant lid mode were present then downwellings would have a very small temperature  
401 contrast of order the rheological temperature scale (Solomatov, 1995) and would therefore be  
402 barely visible or invisible in these plots. Inspection of the viscosity fields indicates a thin  
403 high-viscosity lithosphere; thinner on larger planets as expected from basic scalings (e.g.  
404 Valencia et al., 2007a, van Heck and Tackley, 2011). This mobile lid tectonic mode is not  
405 exactly Earth-like plate tectonics, however: "slabs" seem to aggregate into large-scale highly  
406 viscous downwellings due to the slow, large-scale flow enforced by the high-viscosity post-  
407 perovskite layer.

408

409 Sluggish convection exists in the deep mantles of all planet sizes because the post-perovskite  
410 layers are hot and therefore the viscosity is lower than that predicted along a reference  
411 adiabat: in the range  $10^{22}$ - $10^{28}$  Pa s. Several large-scale hot plumes emanate from a  
412 particularly hot region near the CMB, despite the lack of heat from the core. These large-scale  
413 plumes feed narrow plumes in the perovskite layer (visible particularly in the viscosity field).

414

### 415 3.2.2 Lower bound rheology

416

417 Figure 4 shows temperature and viscosity fields for all five planet sizes and the lower bound  
418 rheology. Again, the existence of downwellings with low temperatures and high viscosities in  
419 all planet sizes indicates that the lithosphere is in a mobile lid, and not stagnant lid, tectonic  
420 mode. The lithosphere is generally strong but with some weak zones, and one or more  
421 subducted "slabs" are visible. In the smaller planets ( $1$ - $3 M_E$ ) the slabs eventually sink to the  
422 deep mantle, but in larger planets they stop before sinking that far, although they do sink into  
423 the post-perovskite layer. In larger planets "slabs" aggregate into large, broad downwellings,  
424 as in the upper-bound cases (Figure 3).

425

426 The thermal structure in the deep mantle changes dramatically with planet size. In small ( $1$ - $3$   
427  $M_E$ ) planets, subducted material sinks to the region above the CMB resulting in a cool,  
428 subadiabatic deep mantle. In the viscosity plot the strong lithosphere, relatively weak upper  
429 mantle, and the cool, higher-viscosity region in the deep mantle are clearly visible. Large ( $5$ -  
430  $10 M_E$ ) planets display quite different behaviour. The deep mantle is very hot - hot enough  
431 that material can flow due to the temperature-dependence of viscosity. Several large plumes  
432 form from this hot material (despite zero net heat flow across the CMB) and rise to the base  
433 of the lithosphere. The deep-mantle viscosity is high, but not as high as it would be along an  
434 adiabatic temperature profile. Slabs pool above this deep high-viscosity region.

435

436 Thus, all size planets have a relatively high viscosity in the deep mantle but for different  
437 reasons. In small planets it is caused by cold slabs pooling, whereas in large planets it is  
438 caused by the intrinsic increase of viscosity with pressure. The deep mantle temperature is  
439 quite different: subadiabatic in small planets but superadiabatic in large planets.

440

### 441 3.2.3 Radial profiles

442

443 These findings are emphasised in profiles of azimuthally-averaged temperature and viscosity  
444 (Figure 5). For upper-bound cases, the temperature in the post-perovskite region is strongly  
445 elevated above the 1800 K adiabat - by around 1000 K near the base of their mantles. As a  
446 result, the azimuthally-averaged viscosity is much lower than that predicted in Figure 1, being  
447 in the range  $10^{25}$ - $10^{26}$  Pa s in most of the pPv layer, but decreasing to  $\sim 10^{24}$  Pa s near the base

448 of the post-perovskite layer. The pPv layer is around 2-3 orders of magnitude more viscous  
449 than the perovskite layer.

450  
451 The lower-bound cases display distinctly different radial profiles, but also with higher than  
452 adiabatic temperatures. Up to  $\sim 300$  GPa, temperature profiles are either adiabatic ( $5-10 M_E$ )  
453 or subadiabatic ( $1-3 M_E$ ). Above 300 GPa, the temperature profile is superadiabatic, following  
454 approximately the same profile for all planet sizes  $5-10 M_E$ , except towards the base of the  
455 largest planets ( $5-10 M_E$ ), where the temperature increases more rapidly. Viscosity profiles  
456 show an increase of viscosity with pressure at lower pressures, but once the viscosity has  
457 reached  $\sim 10^{25}-10^{26}$  Pa s it does not increase any further.

458  
459 Thus, there is a self-regulation of viscosity due to the fact that in equilibrium, each part of the  
460 mantle must be losing its radiogenically-produced heat. If, at some time, the viscosity is too  
461 low (temperature is too high) then convection will be more vigorous and cooling will take  
462 place; on the other hand if viscosity is too high (temperature too low) for the heat to be  
463 advectively lost, then the mantle heats up, reducing the viscosity until material can flow. The  
464 former scenario is more relevant to planetary evolution, as discussed below.

465

466

#### 467 **4. Discussion and conclusions**

468

469 The calculations presented here indicate the dominant influence of rheology on the dynamics  
470 of super-Earth mantles, focussing on potentially habitable super-Earths that have the same  
471 surface conditions as Earth. The rheology used, in particular activation enthalpy as a function  
472 of pressure  $H(p)$ , is based on published DFT calculations for perovskite (Ammann et al.,  
473 2008) and new calculations for post-perovskite (extending (Ammann et al., 2010b)). We  
474 consider rheologies based on both the slowest diffusion direction (upper bound), which  
475 probably dominates diffusion creep, and the fastest diffusion direction (lower bound), which  
476 has been argued to be dominant in dislocation creep (Ammann et al., 2010b). Our convection  
477 calculations show that the deep mantles of large super-Earths ( $7-10 M_E$ ) convect, even if their  
478 viscosity calculated assuming an adiabatic temperature profile is so high that they are  
479 expected not to. This is due to internal heating coupled to the feedback between internal  
480 heating, viscosity and temperature: the deep mantle simply adjusts its temperature such that  
481 its viscosity is the value needed for it to lose its radiogenic heat. A similar self-regulation was  
482 proposed by Tozer (1972) but for the average mantle viscosity; here it applies locally rather  
483 than globally. With the upper-bound viscosity the entire post-perovskite layer is hot, whereas  
484 with the lower-bound viscosity a super-adiabatic temperature profile results. The maximum  
485 azimuthally-averaged viscosity in both cases is in the range  $10^{25}-10^{26}$  Pa s for the parameters  
486 assumed here.

487

488 Analytical theory by (Fowler, 1993) predicted that convection in the limit of strongly  
489 pressure- and temperature- dependent viscosity tends to adopt an isoviscous profile. While  
490 previous numerical convection studies for Earth have not obtained such a profile, we here find  
491 that this theory does indeed apply to very large planets with internal heating. Smaller planets  
492 do not have a sufficiently large viscosity increase along an adiabat for this asymptotic limit to  
493 be reached. Earlier super-Earth calculations with depth-dependent viscosity by (van den Berg  
494 et al., 2010) also did not reach this asymptotic state, instead finding an adiabatic temperature  
495 profile after several billion years of evolution. Recent two-dimensional calculations  
496 (Stamenković, et al., 2012) did obtain a super-adiabatic temperature profile in the case of a  
497 strong increase of activation enthalpy with pressure, similar to our results presented here,  
498 furthermore finding that this state could take a long time to reach depending on the initial  
499 temperature. Recent parameterised studies that use mixing-length theory rather than the usual

500 boundary layer theory to model heat transport in the mantle (Tachinami et al., 2011; Wagner  
501 et al., 2011) also found such a self-regulation effect; their agreement with the full convection  
502 models presented here suggests that mixing length theory is a suitable parameterisation to use  
503 in this situation. Thus, for a pPv rheology that is as realistic, as far as we can calculate and  
504 consistent with some previous studies, a deep stagnant layer cannot form.

505  
506 The present calculations assume a viscosity that is approximately two orders of magnitude  
507 higher than Earth's (at a particular temperature and pressure), in order to properly resolve the  
508 dynamics in the largest planets. This is unlikely to change the basic physics and the trends  
509 observed here but will make some quantitative differences. If the viscosity were two orders of  
510 magnitude lower at every temperature and pressure, a super-Earth's deep mantle would not  
511 have to heat up as much to lose its radiogenic heat. The viscosity would still adjust to  $\sim 10^{25}$ -  
512  $10^{26}$  Pa s, but the temperature would be less super-adiabatic than predicted here.

513  
514 There is, on the other hand, considerable uncertainty in the absolute viscosity of post-  
515 perovskite (of which super-Earth mantles are mainly comprised) due to unknown grain size  
516 and vacancy concentration, and also to the highly anisotropic viscosity. Here we assume that  
517 post-perovskite has a five orders of magnitude higher viscosity than perovskite at Earth deep  
518 mantle convections if the upper bound rheology dominates, or a two orders of magnitude  
519 lower viscosity than perovskite if the lower bound rheology dominates. If it were assumed  
520 that post-perovskite is more viscous, then super-Earth mantles would be hotter; conversely if  
521 we assumed that post-perovskite is less viscous then super-Earth mantles would be less hot. If  
522 dislocation creep is important, then this would tend to reduce the viscosity because, to first  
523 order, power-law rheology can be approximated by linear rheology with an activation  
524 enthalpy reduced by factor  $n$ , the power-law exponent (Christensen, 1984). Another  
525 possibility is that at high pressures the creep mechanism changes to interstitial diffusion and  
526 that this could cause a viscosity reduction with pressure (Karato, 2011), in which case a  
527 super-mantle could be adiabatic. At present there is no quantitative data available to assess  
528 this.

529  
530 Here we focus on calculations that are in thermal equilibrium, with a surface heat flux that  
531 matches the heat input by radiogenic heating, and thus with no secular change in temperature.  
532 We first note that sufficient internal heating (a high Urey ratio) is necessary to obtain the self-  
533 regulation of viscosity observed here. Secondly, in reality planets cool from a hot, and  
534 possibly molten, initial state. Previously it has been found that statistically-steady-state  
535 calculations give a good approximation to the dynamics of cooling-planet calculations (e.g.  
536 the Nu-Ra relationship is the same), except that cooling appears as an additional effective heat  
537 source (e.g. Honda and Iwase, 1996). A prediction of the influence of cooling from a hot  
538 initial state can be found in the models of Tachinami et al (2011), who use mixing-length  
539 theory to predict 1-D profiles of a super-Earth as a function of time. From a hot initial state  
540 they find that the mantle of a  $5 M_E$  super-Earth fairly rapidly (within 1-2 Gyr) adopts a super-  
541 adiabatic profile similar to that found in our lower-bound cases, then changes quite slowly  
542 over subsequent billions of years. The initial adjustment is rapid because convective heat loss  
543 is rapid when the mantle is hot and hence low viscosity. However, subsequent 1-D models  
544 using a different parameterization (Stamenković et al., 2012) found a somewhat longer  
545 adjustment time from a hot initial state, so the question needs to be resolved in the future  
546 using full convection models. Another effect that would influence cooling-planet calculations  
547 is heat conducted from the metallic core, which as a result of core formation is expected to  
548 start super-heated relative to the mantle (Stevenson, 1990).

549  
550 It has been proposed that at early times Earth's mantle had both a shallow magma ocean and a  
551 deep, basal magma ocean (BMO) (Labrosse et al., 2007). Because heat loss from the BMO is

552 controlled by the high-viscosity mantle, the BMO could persist for up to billions of years,  
553 with remnants of it left today as partially-molten ultra-low velocity zones (ULVZs) observed  
554 seismically above the CMB (Lay et al., 2004). Larger planets evolve more slowly with time,  
555 as indicated by parameterised convection models (Kite et al., 2009; Papuc and Davies, 2008).  
556 Because these parameterised models do not account for high viscosity in the deep mantle,  
557 they are likely to overestimate cooling of the deep mantle, which would be slowed by the high  
558 deep-mantle viscosity and resulting high temperatures found here. Therefore, if super-Earths  
559 started off molten, it is plausible that their deep mantles could retain a super-BMO for many  
560 billions of years.

561  
562 Although the present study makes no attempt to systematically study the question of plate  
563 tectonics on super-Earths and we have limited our study to potentially habitable Earth-like  
564 super-Earths, it is notable that mobile-lid behaviour occurs for all planet sizes studied here  
565 while using the same lithospheric yielding parameters (except for the smallest planet where  
566 yield stress had to be decreased) and surface temperature. This is consistent with predictions  
567 from parameterised (Valencia and O'Connell, 2009; Valencia et al., 2007a) and simplified  
568 numerical (Korenaga, 2010a; van Heck and Tackley, 2011) studies. However, it is important  
569 to note that many factors other than planet size influence plate tectonics, including surface  
570 temperature (Lenardic et al., 2008; Landuyt et al., 2009; Foley et al., 2012), the presence of  
571 liquid water (e.g. Regenauer-Lieb et al., 2001), and internal heating rate (O'Neill et al., 2007).  
572 Furthermore, the simple plastic yielding assumed here does not account for history-  
573 dependence of rheology, which may be important for plate tectonics (e.g. Landuyt et al.,  
574 2009; Foley et al., 2012). Clearly, much additional work is needed in order to obtain a  
575 systematic understanding of the likelihood of plate tectonics on super-Earths.

576  
577 Possible breakdown of post-perovskite into constituent oxides as predicted by (Umemoto et  
578 al., 2006) but questioned by (Grocholski et al., 2010) is also not treated here. Currently we  
579 have no estimates of the activation energies in these minerals, so the possible influence on  
580 dynamics is impossible to predict. Metallization of the major minerals is another possibility,  
581 which would not necessarily change activation energies, but would certainly change whether  
582 radiative heat transport is important or not; moreover, heat could then be transported via  
583 electrons. More efficient conductive heat transport would reduce the need for advective heat  
584 transport, allowing viscosities to increase somewhat. There seems to be an indication of a  
585 'last' phase transition within oxide mantles. Mashimo et al. (2006) showed that the transition  
586 to a virtually incompressible oxide  $Gd_3Ga_5O_{12}$  happened after 1.20 Mbars and suggested that  
587 "similar quasi incompressible oxide phases composed of Si, Fe, Mg, and other elements with  
588 relatively high natural abundances, rather than Gd and Ga, might exist in the deep mantles of  
589 large extrasolar rocky planets".

590  
591 The models presented here do not account for chemical differentiation, which is thought to  
592 influence lithospheric dynamics by forming buoyant crust and water-depleted stiff lithosphere  
593 (e.g. (Korenaga, 2010b)), and to influence deep-mantle dynamics by the accumulation of  
594 dense, iron rich material above the CMB (e.g. (Nakagawa and Tackley, 2005a, 2010)). They  
595 also do not include other effects of melting such as magmatic heat transport, which can be an  
596 important heat loss mechanism in early planetary evolution (Nakagawa and Tackley, 2012).

597  
598 In summary, the models presented here can be regarded as a preliminary assessment of the  
599 influence of a realistic activation enthalpy profile on mantle dynamics in super-Earths. The  
600 influences of rheological uncertainties, cooling from a hot initial state, widespread melting,  
601 and differentiation, need to be assessed in future studies in the context of thermo-chemical  
602 evolution of super-Earths.

603

604 **Acknowledgments.** We thank Dave May for helping interface StagYY to PETSc, David  
605 Bercovici and Vlada Stamenković for helpful comments that improved the manuscript, and  
606 Oded Aharonson for his editorial work.  
607  
608

## References

- Ammann, M.W., Brodholt, J.P., Dobson, D.P., 2008. DFT study of migration enthalpies in MgSiO<sub>3</sub> perovskite. *Phys. Chem. Minerals*, doi: 10.1007/s00269-00008-00265-z.
- Ammann, M.W., Brodholt, J.P., Dobson, D.P., 2010a. Simulating diffusion. *Reviews in Mineralogy and Geochemistry* 71, 201-224.
- Ammann, M.W., Brodholt, J.P., Wookey, J., Dobson, D.P., 2010b. First-principles constraints on diffusion in lower-mantle minerals and a weak D" layer. *Nature* 465, 462-465.
- Ammann, M., J. Brodholt, and D. Dobson, 2012. Diffusion of aluminium in MgO from first principles, *Phys. Chem. Miner.* 39(6), 503-514.
- Backus, G.E., 1975. Gross thermodynamics of heat engines in the deep interior of the Earth. *Proc. Natl. Acad. Sci. U.S.A.* 72, 1555-1558.
- Balachandar, S., Yuen, D.A., Reuteler, D., 1992. Time-dependent 3-dimensional compressible convection with depth-dependent properties. *Geophys. Res. Lett.* 19, 2247-2250.
- Balay, S., J. Brown, K. Buschelman, V. Eijkhout, W. D. Gropp, D. Kaushik, M. G. Knepley, L. C. McInnes, B. F. Smith and Hong Zhang, 2012. PETSc Users Manual, ANL-95/11 - Revision 3.3 Argonne National Laboratory.
- Chopelas, A., Boehler, R., 1992. Thermal expansivity in the lower mantle. *Geophys. Res. Lett.* 19, 1983-1986.
- Christensen, U., 1984. Convection with pressure-dependent and temperature-dependent non-Newtonian rheology, *Geophys. J. R. Astron. Soc.*, 77(2), 343-384.
- Davies, G.F., Richards, M.A., 1992. Mantle Convection. *J. Geol.* 100, 151-206.
- Davis, T. A., 2004. Algorithm 832: UMFPACK, an unsymmetric-pattern multifrontal method, *ACM Transactions on Mathematical Software*, 30(2), 196-199.
- de Koker, N., 2010. Thermal conductivity of MgO periclase at high pressure: Implications for the D" region. *Earth Planet. Sci. Lett. (Netherlands)* 292, 392-398.
- Dziewonski, A.M., Anderson, D.L., 1981. Preliminary reference Earth model. *Phys. Earth Planet. Inter.* 25, 297-356.
- Foley, B.J., Bercovici, D., Landuyt, W., 2012. The conditions for plate tectonics on super-Earths: Inferences from convection models with damage. *Earth Planet. Sci. Lett.* 331-332, 281-290.
- Fowler, A.C., 1993. Toward a Description Of Convection With Temperature-and-Pressure-Dependent Viscosity. *Studies In Applied Mathematics* 88, 113-139.
- Goncharov, A.F., Beck, P., Struzhkin, V.V., Haugen, B.D., Jacobsen, S.D., 2009. Thermal conductivity of lower-mantle minerals. *Phys. Earth Planet. Inter.* 174, 24-32.
- Grocholski, B., Shim, S.H., Prakapenka, V.B., 2010. Stability of the MgSiO<sub>3</sub> analog NaMgF<sub>3</sub> and its implication for mantle structure in super-Earths. *Geophys. Res. Lett.* 37, L14204.
- Hansen, U., Yuen, D.A., Kroening, S.E., 1991. Effects Of Depth-Dependent Thermal Expansivity On Mantle Circulations and Lateral Thermal Anomalies. *Geophys. Res. Lett.* 18, 1261-1264.
- Hansen, U., Yuen, D.A., Kroening, S.E., Larsen, T.B., 1993. Dynamic consequences of depth-dependent thermal expansivity and viscosity on mantle circulations and thermal structure. *Phys. Earth Planet. Inter.* 77, 205-223.
- Hernlund, J.W., Tackley, P., 2008. Modeling mantle convection in the spherical annulus. *Phys. Earth Planet. Int.* 171, 48-54.
- Hewitt, J.M., McKenzie, D.P., Weiss, N.O., 1975. Dissipative heating in convective flows. *J. Fluid Mech.* 68, 721-738.
- Hofmeister, A.M., 2008. Inference of high thermal transport in the lower mantle from laser-flash experiments and the damped harmonic oscillator model. *Phys. Earth Planet. Int.* 170, doi: 10.1016/j.pepi.2008.1006.1034.

- Honda, S., and Y. Iwase, 1996. Comparison of the dynamic and parameterized models of mantle convection including core cooling, *Earth Planet. Sci. Lett.*, 139(1-2), 133-145.
- Howard, A.W., Marcy, G.W., Johnson, J.A., Fischer, D.A., Wright, J.T., Isaacson, H., Valenti, J.A., Anderson, J., Lin, D.N.C., Ida, S., 2010. The Occurrence and Mass Distribution of Close-in Super-Earths, Neptunes, and Jupiters. *Science* 330, 653-655.
- Jarvis, G.T., McKenzie, D.P., 1980. Convection in a compressible fluid with infinite Prandtl number. *J. Fluid Mech.* 96, 515-583.
- Jaupart, C., Labrosse, S., Mareschal, J.C., 2007. Temperatures, Heat and Energy in the Mantle of the Earth, in: Editor-in-Chief: Gerald, S. (Ed.), *Treatise on Geophysics*. Elsevier, Amsterdam, pp. 253-303.
- Karato, S., 2011. Rheological structure of the mantle of a super-Earth: Some insights from mineral physics. *Icarus* 212(1), 14-23.
- Karato, S., Wu, P., 1993. Rheology of the upper mantle - a synthesis. *Science* 260, 771-778.
- Karato, S.-i., 2010b. The influence of anisotropic diffusion on the high-temperature creep of a polycrystalline aggregate. *Phys. Earth Planet. Inter.* 183, 468-472.
- Katsura, T., Yoneda, A., Yamazaki, D., Yoshino, T., Ito, E., 2010. Adiabatic temperature profile in the mantle. *Phys. Earth Planet. Inter.* 183, 212-218.
- Kite, E.S., Manga, M., Gaidos, E., 2009. Geodynamics and Rate of Volcanism on Massive Earth-like Planets. *The Astrophysical Journal* 700, 1732.
- Komabayashi, T., Hirose, K., Sugimura, E., Sata, N., Ohishi, Y., Dubrovinsky, L.S., 2008. Simultaneous volume measurements of post-perovskite and perovskite in MgSiO<sub>3</sub> and their thermal equations of state. *Earth Planet. Sci. Lett.* 265, 515-524.
- Korenaga, J., 2010a. On the likelihood of plate tectonics on super-Earths: Does size matter? *Astrophys. J. Lett.* 725, L43-L46.
- Korenaga, J., 2010b. Scaling of plate-tectonic convection with pseudoplastic rheology. *J. Geophys. Res.* 115, doi:10.1029/2010JB007670.
- Labrosse, S., Hernlund, J.W., Coltice, N., 2007. A crystallising dense magma ocean at the base of Earth's mantle. *Nature* 450, 866-869.
- Landuyt, W., Bercovici, D., 2009. Variations in planetary convection via the effect of climate on damage. *Earth Planet. Sci. Lett.* 277, 29-37.
- Lay, T., Garnero, E.J., Williams, Q., 2004. Partial melting in a thermo-chemical boundary layer at the base of the mantle. *Phys. Earth Planet. Int.* 146, 441-467.
- Lenardic, A., Jellinek, A.M., Moresi, L.N., 2008. A climate induced transition in the tectonic style of a terrestrial planet. *Earth Planet. Sci. Lett.* 271, 34-42.
- Mashimo, T., R. Chau, Y. Zhang, T. Kobayoshi, T. Sekine, K. Fukuoka, Y. Syono, M. Kodama, and W. J. Nellis, 2006. Transition to a virtually incompressible oxide phase at a shock pressure of 120 GPa (1.2 mbar), Gd<sub>3</sub>Ga<sub>5</sub>O<sub>12</sub>. *Phys. Rev. Lett.*, 96(10), 105504, 1-4.
- Moresi, L., Solomatov, V., 1998. Mantle convection with a brittle lithosphere - Thoughts on the global tectonic styles of the Earth and Venus. *Geophys. J. Int.* 133, 669-682.
- Mosenfelder, J.L., Asimow, P.D., Frost, D.J., Rubie, D.C., Ahrens, T.J., 2009. The MgSiO<sub>3</sub> system at high pressure: Thermodynamic properties of perovskite, postperovskite, and melt from global inversion of shock and static compression data. *J. Geophys. Res.* 114, B01203.
- Nakagawa, T., Tackley, P.J., 2005a. Deep mantle heat flow and thermal evolution of Earth's core in thermo-chemical multiphase models of mantle convection. *Geochem., Geophys., Geosys.* 6, doi:10.1029/2005GC000967.
- Nakagawa, T., Tackley, P.J., 2005b. The interaction between the post-perovskite phase change and a thermo-chemical boundary layer near the core-mantle boundary. *Earth Planet. Sci. Lett.* 238, 204-216.
- Nakagawa, T., Tackley, P.J., 2010. Influence of initial CMB temperature and other parameters on the thermal evolution of Earth's core resulting from thermo-chemical

- spherical mantle convection. *Geophys. Geochem. Geosyst.* 11, doi:10.1029/2010GC003031.
- Nakagawa, T., Tackley, P.J., 2011. Effects of low-viscosity post-perovskite on thermo-chemical convection in a 3-D spherical shell. *Geophys. Res. Lett.* 38, doi:10.1029/2010GL046494.
- Nakagawa, T., and P. J. Tackley (2012), Influence of magmatism on mantle cooling, surface heat flow and Urey ratio, *Earth Planet. Sci. Lett.*, 329-330, 1-10.
- O'Neill, C., Lenardic, A., 2007. Geological consequences of super-sized Earths. *Geophys. Res. Lett.* 34, doi:10.1029/2007GL030598.
- O'Neill, C., Lenardic, A., Moresi, L., Torsvik, T.H., Lee, C.T.A., 2007. Episodic Precambrian subduction. *Earth Planet. Sci. Lett.* 262, 552-562.
- Papuc, A.M., Davies, G.F., 2008. The internal activity and thermal evolution of Earth-like planets. *Icarus* 195, 447-458.
- Regenauer-Lieb, K., Yuen, D.A., Branlund, J., 2001. The initiation of subduction: Criticality by addition of water? *Science* 294, 578-580.
- Schubert, G., Turcotte, D.L., Olson, P., 2000. *Mantle Convection in the Earth and Planets.* Cambridge University Press.
- Seager, S., Kuchner, M., Hier-Majumder, C.A., Militzer, B., 2007. Mass-radius relationships for solid exoplanets. *Astrophys. J.* 669, 1279-1297.
- Solomatov, V. S., 1995. Scaling of temperature-dependent and stress-dependent viscosity convection, *Phys. Fluids*, 7(2), 266-274.
- Sotin, C., Grasset, O., Mocquet, A., 2007. Mass–radius curve for extrasolar Earth-like planets and ocean planets. *Icarus* 191, 337-351.
- Stamenković, V., Breuer, D., Spohn, T., 2011. Thermal and transport properties of mantle rock at high pressure: Applications to super-Earths. *Icarus* 216, 572-596.
- Stamenković, V., Noack, L., Breuer, D., Spohn, T., 2012. The Influence of Pressure-dependent Viscosity on the Thermal Evolution of Super-Earths. *The Astrophysical Journal* 748, 41.
- Stevenson, D.J., 1990. Fluid dynamics of core formation, in: Newman, H.E., Jones, J.H. (Eds.), *Origin of the Earth.* Oxford University Press, pp. 231-249.
- Tachinami, C., Senshu, H., Ida, S., 2011. Thermal Evolution and Lifetime of Intrinsic Magnetic Fields of Super-Earths in Habitable Zones. *The Astrophysical Journal* 726, 70.
- Tackley, P.J., 2000. Self-consistent generation of tectonic plates in time-dependent, three-dimensional mantle convection simulations Part 2: Strain weakening and asthenosphere. *Geochem., Geophys., Geosys.* Volume 1, Paper number 2000GC000043 [000014,000420 words, 000015 figures, 000041 table].
- Tackley, P.J., 2008. Modelling compressible mantle convection with large viscosity contrasts in a three-dimensional spherical shell using the yin-yang grid. *Phys. Earth Planet. Int.*, doi:10.1016/j.pepi.2008.1008.1005.
- Tackley, P.J., Xie, S., 2003. Stag3D: A code for modeling thermo-chemical multiphase convection in Earth's mantle, *Second MIT Conference on Computational Fluid and Solid Mechanics.* Elsevier, MIT, pp. 1-5.
- Tozer, D.C., 1972. The present thermal state of the terrestrial planets. *Phys. Earth Planet. Inter.* 6, 182-197.
- Trompert, R., Hansen, U., 1998. Mantle convection simulations with rheologies that generate plate-like behavior. *Nature (UK)* 395, 686-689.
- Umemoto, K., Wentzcovitch, R.A., Allen, P.B., 2006. Dissociation of MgSiO<sub>3</sub> in the cores of gas giants and terrestrial exoplanets. *Science* 311, 983-986.
- Valencia, D., O'Connell, R.J., 2009. Convection scaling and subduction on Earth and super-Earths. *Earth Planet. Sci. Lett.* 286, 492-502.



- Valencia, D., O'Connell, R.J., Sasselov, D., 2006. Internal structure of massive terrestrial planets. *Icarus* 181, 545-554.
- Valencia, D., O'Connell, R.J., Sasselov, D.D., 2007a. Inevitability of plate tectonics on super-Earths. *Astrophys. J.* 670, L45-L48.
- Valencia, D., O'Connell, R., Sasselov, D., 2009. The role of high-pressure experiments on determining super-Earth properties. *Astrophysics and Space Science* 322, 135-139.
- Valencia, D., Sasselov, D., O'Connell, R.J., 2007b. Radius and structure models of the first super-Earth planet. *Astrophys. J.* 656, 545-551.
- Valencia, D., Sasselov, D.D., O'Connell, R.J., 2007c. Detailed models of super-Earths: How well can we infer bulk properties? *Astrophys. J.* 665, 1413-1420.
- van den Berg, A.P., Yuen, D.A., Beebe, G.L., Christiansen, M.D., 2010. The dynamical impact of electronic thermal conductivity on deep mantle convection of exosolar planets. *Phys. Earth Planet. Inter.* 178, 136-154.
- van Heck, H., Tackley, P.J., 2011. Plate tectonics on super-Earths: Equally or more likely than on Earth. *Earth Planet. Sci. Lett.* 310, 252-261.
- Wagner, F.W., Sohl, F., Hussmann, H., Grott, M., Rauer, H., 2011. Interior structure models of solid exoplanets using material laws in the infinite pressure limit. *Icarus* 214, 366-376.

## **Figure Captions**

**Figure 1.** (Top): Activation enthalpy as a function of pressure for perovskite and post-perovskite. The points are from the Density Functional Theory of Ammann et al (2009) for perovskite and Ammann et al. (2010) and the present study for post-perovskite. The lines are the analytical fits. (Middle): Viscosity profile along the 1600 K adiabat for the upper-bound rheology. (Bottom) Viscosity profile along the 1600 K adiabat for the lower-bound rheology.

**Figure 2.** Pressure-dependence of density, thermal expansivity and thermal conductivity, and the resulting 1600 K adiabat, as labelled.

**Figure 3.** Representative viscosity (left column) and temperature (right column) fields for the upper-bound rheology and all five planet sizes. For clearer visualization the viscosity is truncated at  $10^{28}$  Pa s, which is lower than the  $10^{40}$  Pa s truncation used in the numerical calculations.

**Figure 4.** Representative viscosity (left column) and temperature (right column) fields for the lower-bound rheology and all five planet sizes. For clearer visualization the viscosity is truncated at  $10^{28}$  Pa s, which is lower than the  $10^{40}$  Pa s truncation used in the numerical calculations.

**Figure 5.** Profiles of azimuthally-averaged temperature and viscosity for five planet sizes, as labelled. The arithmetic average is used for temperature and the geometric average for viscosity. In the temperature, the 1800 K adiabat is also plotted.

## Tables

Pressure (GPa)	$\eta_0^{low}$	$H^{low}$ (eV)	$\eta_0^{high}$	$H^{high}$ (eV)
131.6	$2185 \times 10^{30}$	3.4	$40 \times 10^{30}$	10.3
505.4	$1245 \times 10^{30}$	7.1	$95 \times 10^{30}$	14.0
1016.1	$945 \times 10^{30}$	9.6	$180 \times 10^{30}$	15.2

**Table 1:** Quantities required for the viscosity of MgSiO<sub>3</sub> post-perovskite.

Mineralogy	$E_0$ (kJ/mol)	$V_0$ (cm <sup>3</sup> /mol)	$p_{decay}$ (GPa)	$\eta_0$ (Pa s)
“upper mantle”	300	5.00	$\infty$	$10^{21}$
perovskite	370	3.65	200	$3.00 \times 10^{23}$
post-perovskite lower bound	162	1.40	1610	$1.90 \times 10^{21}$
post-perovskite upper bound	780	1.70	1100	$1.05 \times 10^{34}$

**Table 2.** Parameters for H(p) analytical fit (equations (2)-(4)).

Mineralogy	$K_0$ (GPa)	$K'$	$\gamma_0$
“upper mantle”	163	4.0	1.3
“transition zone”	85	4.0	0.85
“perovskite”	210	3.9	1.3
“post-perovskite”	210	3.9	1.3

**Table 3.** Fit of Birch-Murnaghan equation of state parameters for four mantle mineralogies, plus assumed zero-pressure Gruneisen parameter.

Property	Symbol	Value	Units
Conductivity: surface	$k_0$	3.0	W/m-K
Heat Capacity	$C_p$	1200	J/kg-K
Surface temperature	$T_{surf}$	300	K
Internal heating rate	$H$	$5.2 \times 10^{-12}$	W/kg
Friction coefficient	$c_f$	0.1	-
Yield stress (p=0)	$\sigma_{duct}$	50 (1 $M_E$ ) 100 (3-10 $M_E$ )	MPa
Yield stress pressure gradient	$\sigma'_{duct}$	0.01	-

**Table 4.** Values of various constant properties.

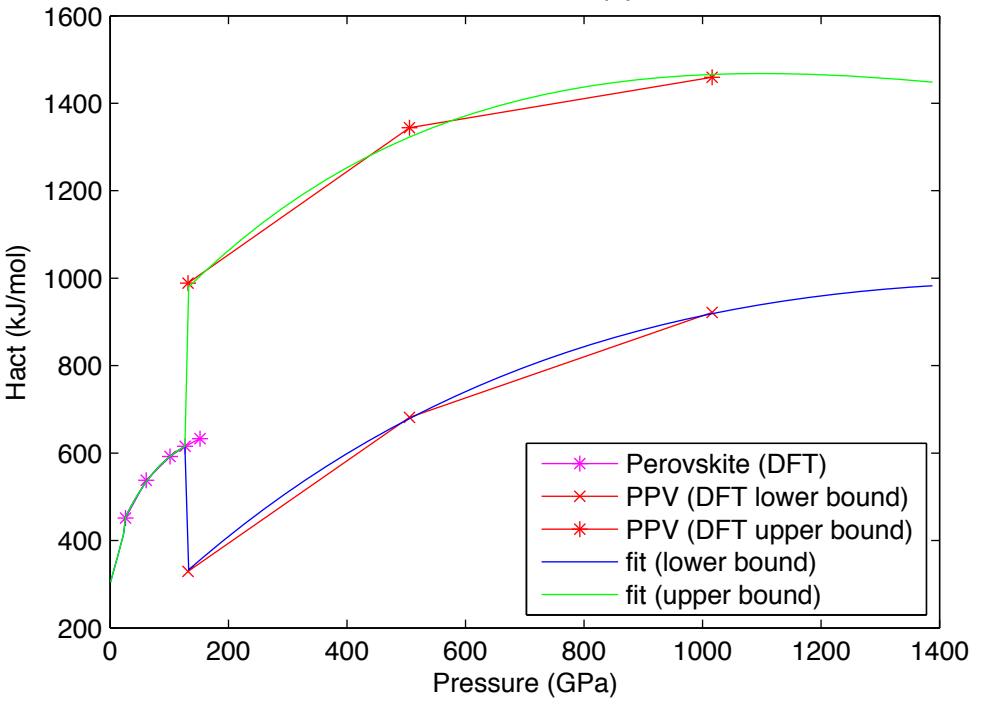
$M/M_E$	<b>R (km)</b>	<b>R<sub>cmb</sub> (km)</b>	<b><math>\langle g \rangle_{\text{mantle}}</math> (m/s<sup>2</sup>)</b>	<b>P<sub>cmb</sub> (GPa)</b>
3	8578.0	4602.1	16.996	388.4
5	9823.6	5186.8	22.062	657.9
7	10703	5597.6	26.382	944.5
10	11683	6063.5	32.076	1400

**Table 5.** Calculated dimensions and mean gravitational acceleration of the mantle as a function of planet mass.

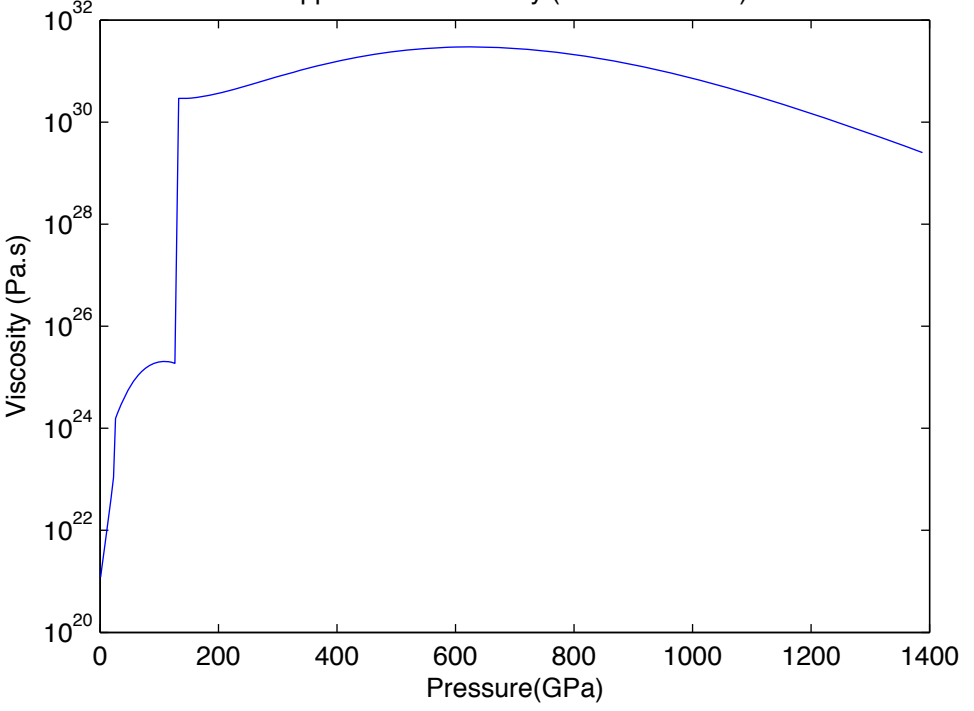
<b>Depth (km)</b>	<b>Temperature (K)</b>	<b><math>\Delta\rho</math> (kg/m<sup>3</sup>)</b>
<i>Olivine-Spinel-Perovskite-Postperovskite</i>		
410	1600	280
660	1900	400
2740	2650	60
<i>Pyroxene-Garnet-Perovskite-Postperovskite</i>		
60	0	350
400	1600	100
720	1900	500
2700	2650	60

**Table 6.** Phase transitions and properties. All Clapeyron slopes are set to 0

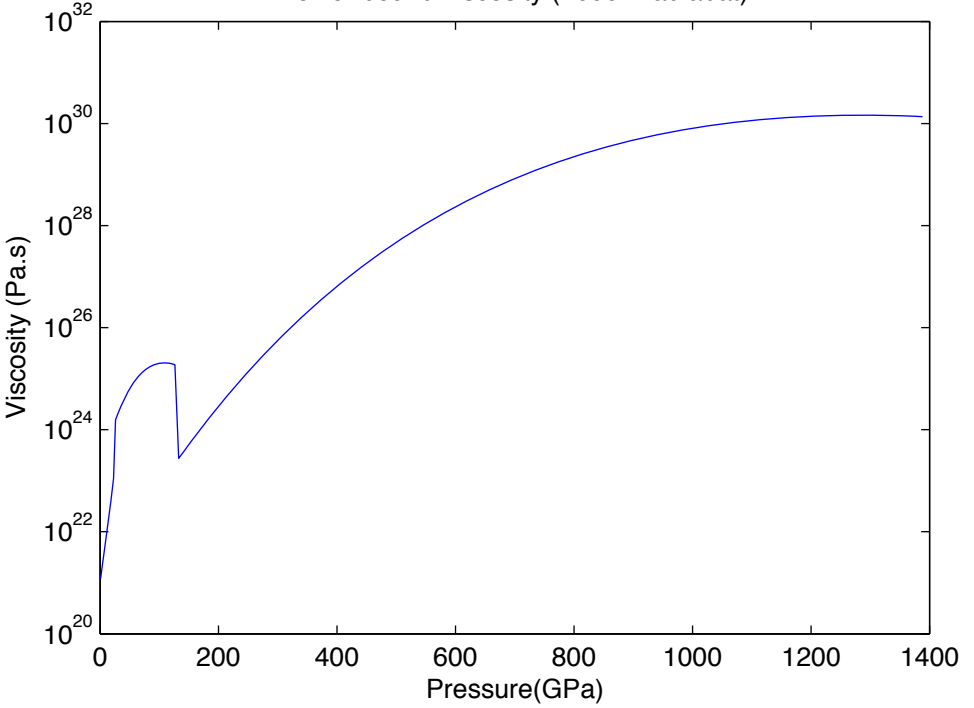
Activation Enthalpy

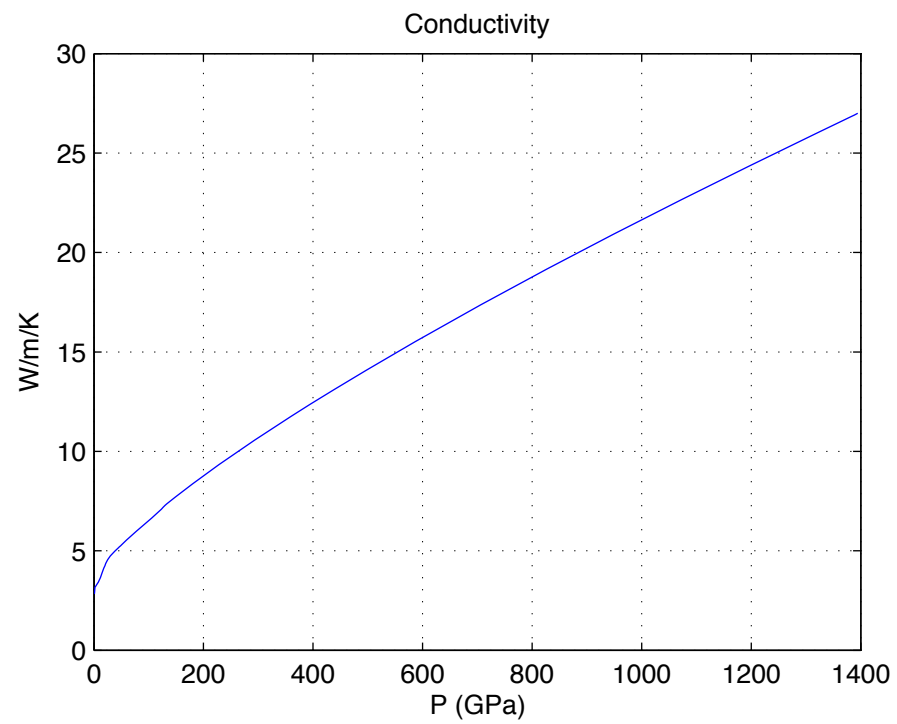
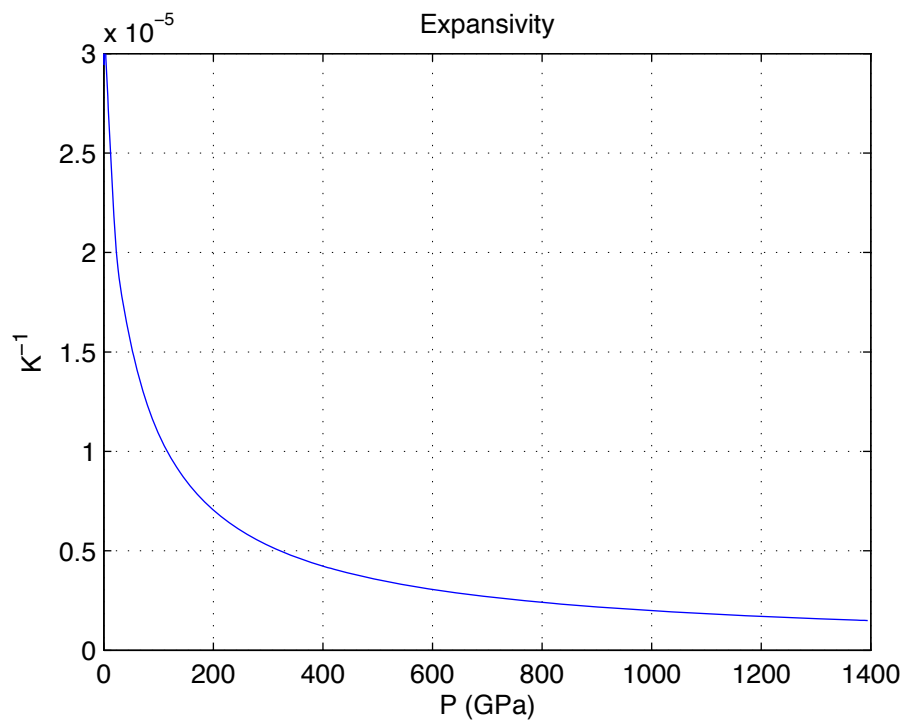
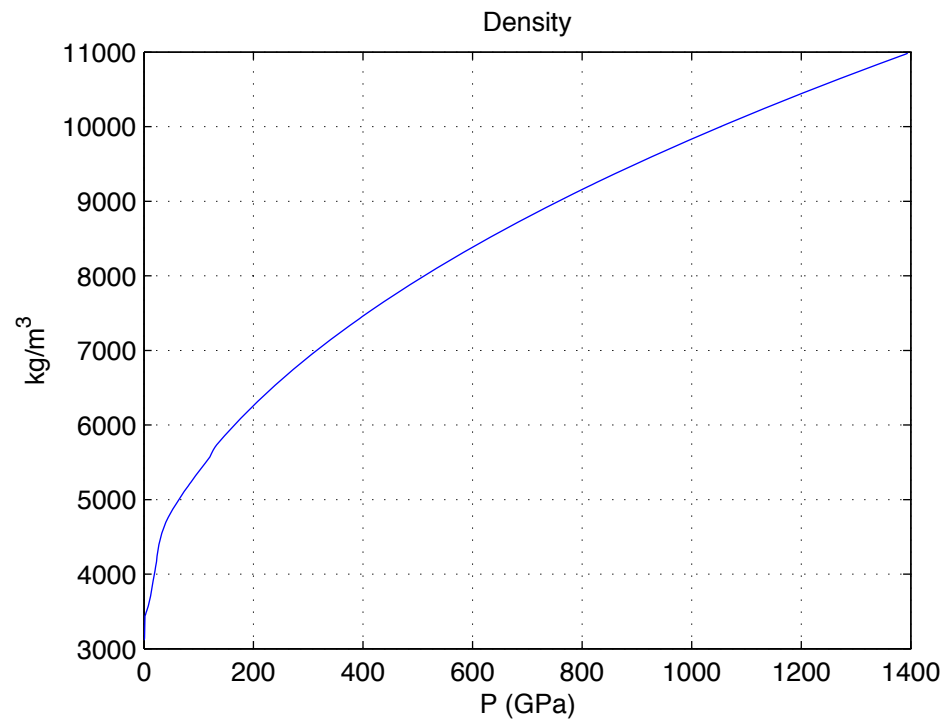
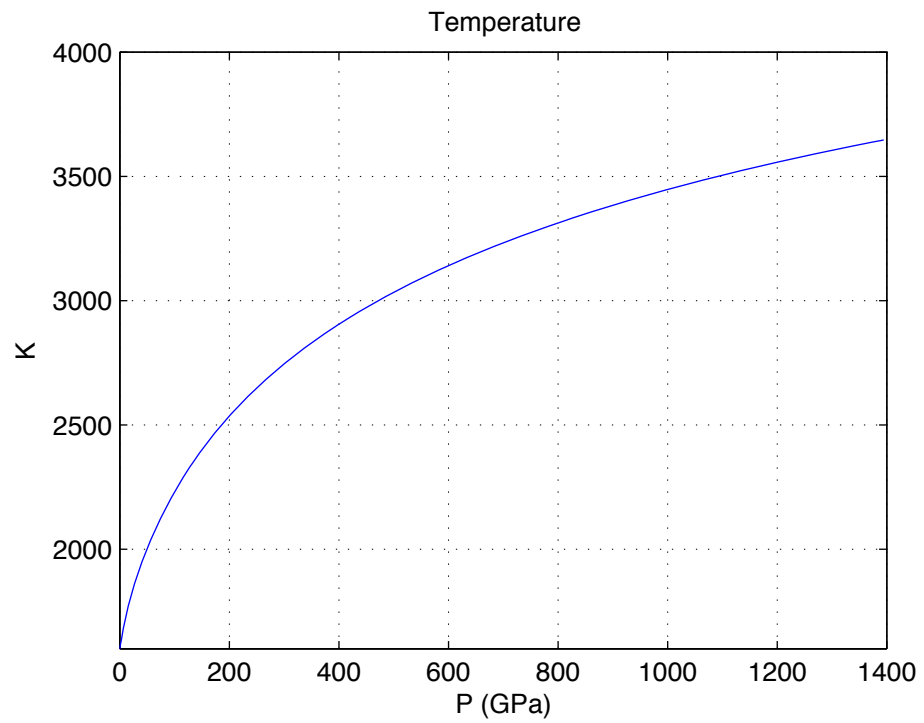


Upper bound viscosity (1600 K adiabat)

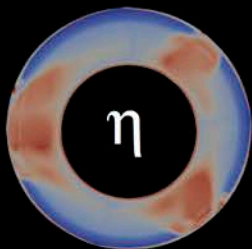


Lower bound viscosity (1600 K adiabat)

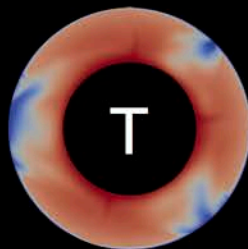




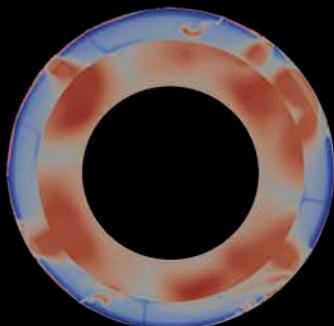
Viscosity  
 $1e+28$   
 $1e+26$   
 $1e+24$   
 $1e+22$   
 $1e+20$   
 $1e+19$



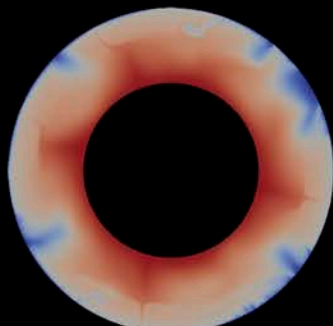
1 M<sub>E</sub>



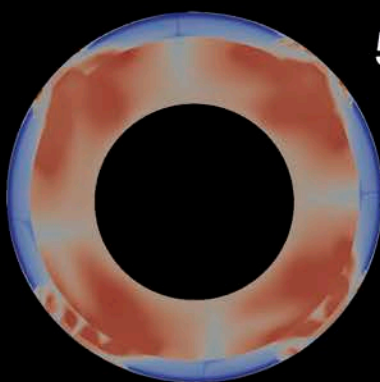
T  
2900  
2000  
1000  
300



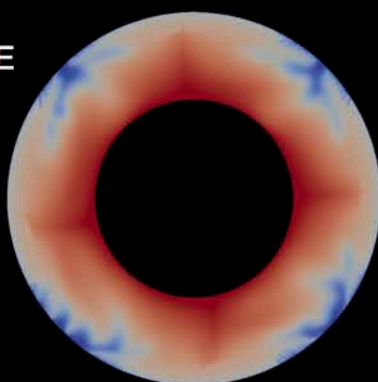
3 M<sub>E</sub>



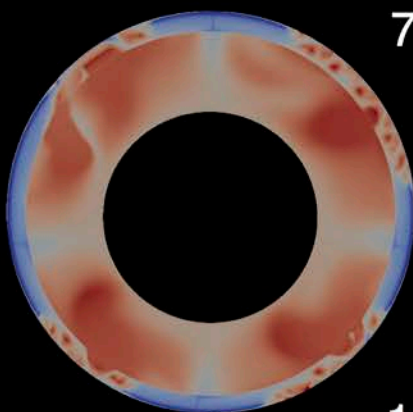
T  
4200  
4000  
3000  
2000  
1000  
300



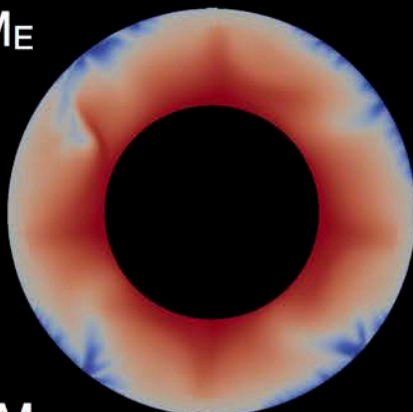
5 M<sub>E</sub>



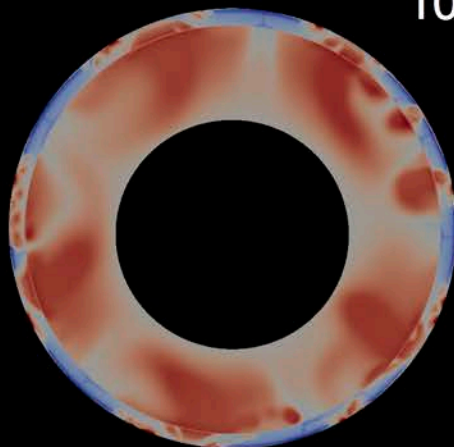
T  
4600  
4000  
3000  
2000  
1000  
300



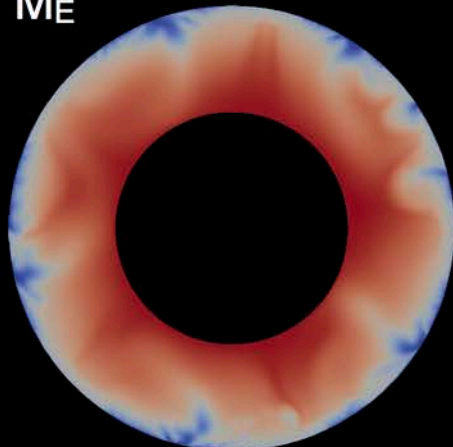
7 M<sub>E</sub>



T  
4900  
4000  
3000  
2000  
1000  
300

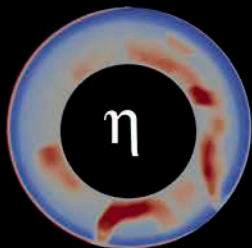


10 M<sub>E</sub>

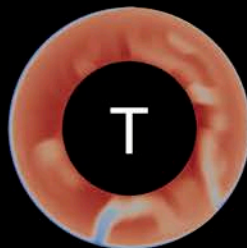


T  
5100  
5000  
4000  
3000  
2000  
1000  
300

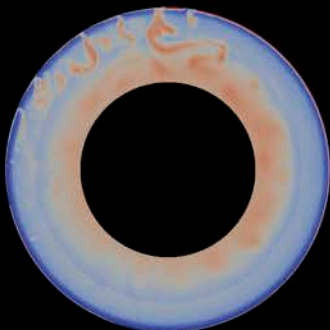
Viscosity  
1e+28  
1e+26  
1e+24  
1e+22  
1e+20  
1e+19



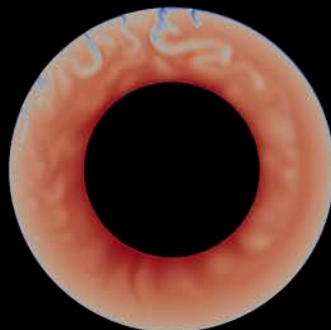
1 M<sub>E</sub>



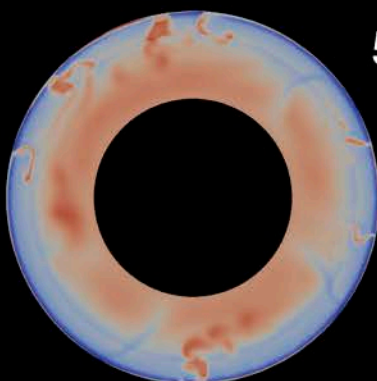
T  
2800  
2000  
1000  
300



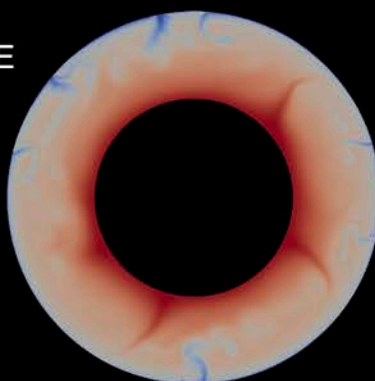
3 M<sub>E</sub>



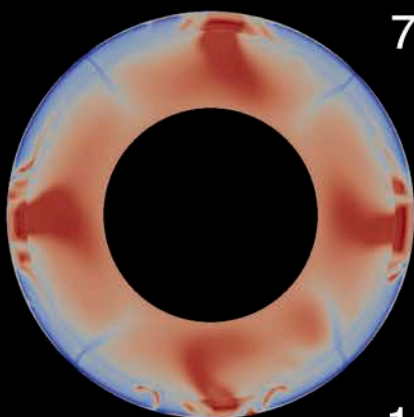
T  
3700  
3000  
2000  
1000  
300



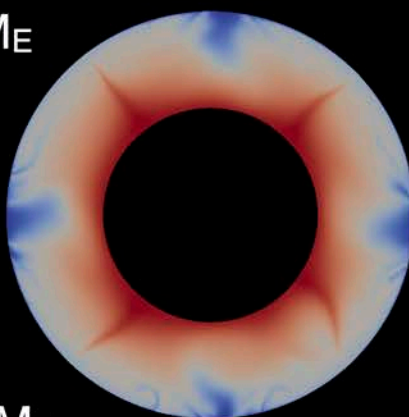
5 M<sub>E</sub>



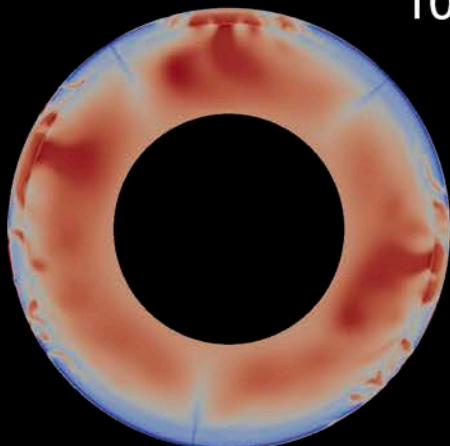
T  
4600  
4000  
3000  
2000  
1000  
300



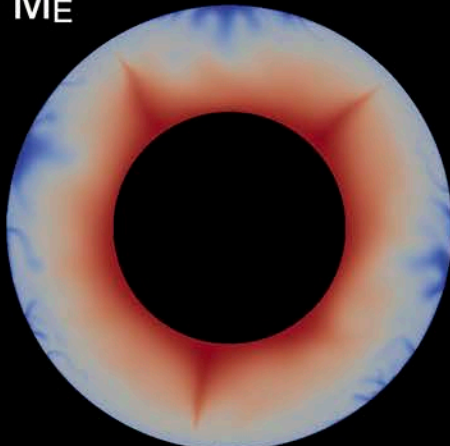
7 M<sub>E</sub>



T  
5200  
5000  
4000  
3000  
2000  
1000  
300



10 M<sub>E</sub>



T  
5900  
5000  
4000  
3000  
2000  
1000  
300



